
Proceedings Paper:
Moussa, A. and Liu, W. orcid.org/0000-0003-2968-2888 (2023) Enhanced detection in automotive applications using bistatic radar with cooperative roadside sensors. In: Proceedings of CIE International Conference on Radar (Radar 2021). CIE International Conference on Radar (Radar 2021), 15-19 Dec 2021, Haikou, Hainan, China.. Institute of Electrical and Electronics Engineers , pp. 1649-1653. ISBN 978-1-6654-9814-2

https://doi.org/10.1109/Radar53847.2021.10028039

Enhanced Detection in Automotive Applications Using Bistatic Radar with Cooperative Roadside Sensors

1st Ali Moussa
Department of Electronic and Electrical Engineering
The University of Sheffield
Sheffield, UK
amoussa1@sheffield.ac.uk

2nd Wei Liu
Department of Electronic and Electrical Engineering
The University of Sheffield
Sheffield, UK
w.liu@sheffield.ac.uk

***Abstract*—The state-of-art automotive radar modules normally operate in the monostatic mode and little research has been done on the ability of a vehicle to operate such application when the transmitter is located externally, a setup commonly referred to as bistatic mode. Our proposal here is to combine the communication potential of fifth-generation (5G) new radio (NR) with the merits of bistatic radar to advance the existing automotive radar technology. This application can be envisioned in a smart highway where a vehicle switches to an economic mode, and the long-range radar modules rely on cooperative roadside transmitters (communicating via pre-determined protocols) to locate targets in its vicinity. Computer simulations show that this proposed application can outperform the monostatic equivalent.**

***Index Terms*—Automotive radar, bistatic radar, radar signal processing.**

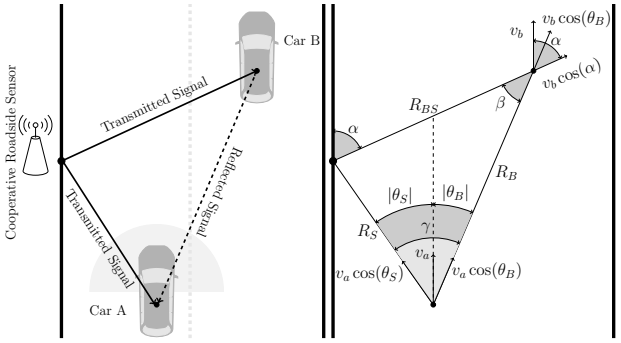

Fig. 1. Geometry of the automotive bistatic passive localisation scenario.

I. Introduction

Radar based sensing is a key enabling technology for autonomous driving and future intelligent transportation systems [1], and recently the automotive industry has benefited significantly from the development of various millimetre wave radar technologies, deployed for applications such as adaptive cruise control (ACC), parking assistance (PA), autonomous emergency brake (AEB), advanced driver assistance systems (ADAS), etc [2]. Naturally, the focus of automotive radar has been on the monostatic mode, i.e. the radar is equipped with its own transmitters and receivers for effective target detection and estimation, given the simplicity of its implementation and processing.

On the contrary, a passive bistatic radar relies on a transmitter typically located far away from the receiver, and requires an additional reference receiver for collecting a direct-path signal needed for the de-modulation task [3]. Without loss of generality, any form of communication between the transmitter and the receiver that allows instantaneous sharing of the modulation parameters of the transmitted waveform, as well as tight time synchronisation, is sufficient for the operation of such radar systems. In fact, despite being dominated by the pros of the monostatic radar, the bistatic variation resurged in the 1990s with more research drawn into bistatic synthetic-aperture-radar (SAR), remote sensing, and stealthy detection [4]–[9], etc. However, it has since then struggled to break into the automotive industry, partly due to the very strict synchronisation requirements (at least 1ns). Nonetheless, motivated by the drive in the fifth-generation (5G) communication and beyond to meet the requirements of vehicular applications (emphasised in [10], [11]), especially the stringent synchronisation, new prospects for bistatic radar application could be forming.

In this work, an application of bistatic radar in an automotive scenario that incorporates cooperative roadside sensors is proposed. Suppose that on a highway, there exist one stationary roadside sensor transmitting radar waveforms, and one traveling vehicle passively relying on these signals to locate other cars ahead of it in a bistatic manner. The idea is to relieve the vehicle from the transmission task, which inherently reduces power consumption. This also extends the detectable range of the vehicle's front long-range radar when the targets are closer to the roadside sensor than the receiving antenna. Fig. 1 shows a schematic of such a scenario, where car A acts as a passive receiver and aims to locate car B using signals transmitted by the roadside sensor. Being of a cooperative nature, the latter transmits a modulated waveform suitable for radar applications – typically a frequency modulated continuous wave (FMCW) – and informs car A of its transmission routine and

This work is supported by the UK Engineering and Physical Sciences Research Council (EPSRC) under grants EP/T517215/1 and EP/V009419/1.

modulation parameters via a 5G link with an agreed protocol. Although sharing such information is straightforward and can be achieved using vehicle-to-infrastructure (V2I) communications [12], meeting the synchronisation requirements can be a critical task. Briefly, this synchronisation task between the searching car and the roadside sensor can be achieved by fixing both local clock units to the same time reference, with an acceptable offset. It is important to mention, however, that in the proposed application, the synchronisation requirements, and the possible prospects to meeting them differ from that in bistatic vehicular applications exploiting 5G new-radio (NR) waveforms between multiple nodes ([13] for instance). This adds another element of novelty to this work as emerging applications always drove specific synchronisation requirements [14]. Here we can state the following: the searching vehicle can be synchronised by a local time reference present at the roadside sensor (no need for coordinated-universal-time (UTC) as a discipline); a clear line-of-sight (LOS) is available between the sensor and the vehicle; the latter can both have time reference units of the same granularity and specifications; the roadside sensor can quantify its clock drift due to its synchronisation to the Global Navigation Satellite System (GNSS) atomic clock, and can communicate its drift to the vehicle after the initial synchronisation (as long as the drift does not exceed the latency of the communication link); the minimum accepted clock offset is dictated by the range resolution of bistatic FMCW radar and is independent from GNSS localisation accuracy and the instantaneous motion parameters of the vehicle; the searching vehicle can have private access to GNSS, adding to the degrees of freedom available for the synchronisation task.

In the rest of this paper, the geometry of the proposed application alongside its solution is provided in Sec. II. Then, the bistatic FMCW signal model is presented in Sec. III, followed by performance analysis in Sec. IV. A parameter estimation/processing algorithm based on fast Fourier transform (FFT) is proposed in Sec. V. Finally, simulations are presented in Sec. VI, and conclusions drawn in Sec. VII.

II. Solution to the Geometry of The Proposed Scenario

Assume car A is using the signals transmitted by the roadside sensor to locate car B, by estimating its range, Doppler and direction of arrival (DOA), denoted by R_B, v_b and θ_B, respectively. Let R_S and R_{BS} be the distances between the sensor and cars A and B, respectively, v_a the velocity of car A, and θ_S the DOA of the sensor. By applying the cosine law to the angle γ in Fig. 1, we have

$$R_{BS}^2 = R_B^2 + R_S^2 - 2R_B R_S \cos(\gamma), \tag{1}$$

where γ is an auxiliary angle and can be defined as

$$\gamma = |\theta_S - \theta_B|. \tag{2}$$

From Fig. 1, the multipath signal transmitted by the sensor travels a distance

$$R_m = R_{BS} + R_B, \tag{3}$$

before it reaches car A. Combining (1) and (3) leads to the following

$$R_B = \frac{R_m^2 - R_S^2}{2R_m - 2R_S\cos(\gamma)}. \tag{4}$$

Assume cars A and B are moving with constant speed over the considered period of signal transmission, and that their motion is purely forward such that car A is approaching the sensor and car B is receding from it. The velocity projected on the direct-path signal due to the motion of car A can be defined as

$$V_d = -v_a \cos(\theta_S). \tag{5}$$

Similarly, the velocity projected on each path of the multi-path signal can be defined as

$$V_m = v_b \cos(\alpha) + (v_b - v_a)\cos(\theta_B), \tag{6}$$

where α is an auxiliary angle and can be defined using the sine law as

$$\alpha = \arcsin\left(\frac{R_S}{R_m - R_B}\sin(\gamma)\right) + \theta_B. \tag{7}$$

By combining (6) and (7), v_b can be calculated as

$$v_b = \frac{V_m + v_a\cos(\theta_B)}{\cos(\alpha) + \cos(\theta_B)}. \tag{8}$$

To solve this geometry problem, R_m, R_S, V_m ,V_d, θ_B, and θ_S should be known. Next, we show how the latter can be unambiguously estimated.

III. FMCW Bistatic Radar Signal Model

Suppose that at time $t_0 = 0$, the roadside sensor transmits a frame of periodic FMCW signals, known as chirps. Each frame contains M chirps transmitted with repetition interval T. A normalised single transmitted frame can be represented in the complex form as

$$s(t) = \begin{cases} e^{j2\pi(f_0 t + 0.5\mu t^2)} & t \in [t_0 + mT, t_0 + mT + T_c), \\ 0 & \text{otherwise}, \end{cases} \tag{9}$$

where $\mu = \frac{B}{Tc}$, B, and T_c denote the modulation rate, bandwidth, and period, respectively. f_0 is the starting frequency, t is the continuous real time, and $m = 0, 1, \ldots, M-1$ is the chirp index.

Assuming no path loss, the direct-path signal received at car A can be expressed as

$$r_d(t) = s(t - \tau_d(t)) = e^{j2\pi(f_0(t-\tau_d(t)) + 0.5\mu(t-\tau_d(t))^2)}, \tag{10}$$

where $\tau_d(t) = \frac{R_S}{c} + \frac{V_d}{c}t$.

It is clear that the starting time stamp of the received signal r_d varies with time due to motion of the vehicles, so it makes sense to decompose the real time domain t into fast time t_f and slow time mT such that $t = t_f + mT$ and $t_f \in [t_0, t_0 + T_c)$. Consequently, $r_d(t)$ becomes

$$r_d(m, t_f) = e^{j2\pi(f_0(t_f + mT - \tau_d(m,t_f)) + 0.5\mu(t_f + mT - \tau_d(m,t_f))^2)}, \tag{11}$$

and $\tau_d(m,t_f) = \frac{R_S}{c} + \frac{V_d}{c}(t_f + mT)$. Similarly, the multi-path signal received at car A can be written as

$$r_m(m,t_f) = e^{j2\pi(f_0(t_f+mT-\tau_m(m,t_f))+0.5\mu(t_f+mT-\tau_m(m,t_f))^2)}, \tag{12}$$

where $\tau_m(m,t_f) = \frac{R_m}{c} + \frac{V_m}{c}(t_f + mT)$. The signal received at car A is now a superposition of both paths, i.e.

$$y(m,t_f) = r_d(m,t_f) + r_m(m,t_f). \tag{13}$$

To extract the embedded information, the received signal is cross-correlated with a signal identical to the one in (9) generated locally. Here, we assume perfect synchronisation, and that the modulation settings are known. Since the transmitted chirps are periodic, they do not vary across the slow time and can be simplified to

$$s_o(t_f) = s(t_f)_{m=0} = e^{j2\pi(f_c t_f + 0.5\mu t_f^2)}. \tag{14}$$

The same simplification can also be applied to the reflected signals. After sampling the fast time at rate f_s, the sampled de-chirped signal can be written as

$$z(m,n) = y(m,n)s(m,n)^*, \tag{15}$$

where $(.)^*$ is the complex conjugate, $n = 0, 1, \ldots, N-1$ is the sampling index, and $N = f_s T_c$ is the total number of fast-time samples.

Suppose that car A is equipped with a uniform linear array (ULA) of L antennas with adjacent distance d [15]. After some Mathematical expansion and simplifications, the sampled de-chirped signal can now be defined as a function of slow time, fast time, and antenna element as

$$\begin{aligned} &z(m,n,l) \\ &= \exp[-j2\pi(f_0\frac{R_S}{c} + \mu\frac{R_S}{c}\frac{n}{f_s} + f_0\frac{V_d}{c}mT + \frac{f_0 d\sin\theta_S}{c}l)] \\ &+ \exp[-j2\pi(f_0\frac{R_m}{c} + \mu\frac{R_m}{c}\frac{n}{f_s} + f_0\frac{V_m}{c}mT + \frac{f_0 d\sin\theta_B}{c}l)], \end{aligned} \tag{16}$$

where $l = 0, 1, \ldots, L-1$ is the antenna index.

Taking into account the Nyquist considerations, the maximum unambiguous multi-path range can be modelled as

$$\mathcal{R} = \frac{cf_s}{\mu}. \tag{17}$$

Assuming the observation period in the fast-time domain is equal to the chirp duration, the Rayleigh resolution of the direct-path and multi-path range can be modelled respectively as

$$\delta_{R_d} = \frac{c}{B}, \qquad \delta_{R_m} = \frac{c}{2B\cos(\beta/2)}, \tag{18}$$

where $\beta = \alpha - \theta_B$ is the bistatic angle.

IV. Performance Analysis

Assuming free-space propagation and same radar parameters, using the radar range equation, we can derive the following relationship between the maximum detectable range of car B from car A (denoted by $R_{B_{\max}}$) in this proposed application, and that of a typical monostatic radar (denoted by $R_{\max}$)

$$R_{B_{\max}} = \sqrt{\frac{\sigma_{\text{bi}}}{\sigma_{\text{mono}}}}\frac{R_{\max}^2}{R_{BS}} \tag{19}$$

where σ_{bi} and σ_{mono} denote the bistatic and monostatic radar cross section (RCS), respectively. Assuming they are equal, it is clear that car A can detect car B at much further distances using the proposed bistatic radar when it is closer to the roadside sensor than to car B (i.e. $R_{BS} < R_B$). This is shown in Fig. 2 where $R_{\max}$ is set to 100m, typically achieved by existing automotive monostatic radar for front applications. In reality, the roadside sensor can have much higher transmission power and gain than the radar module fitted in the car, thereby improving the detection range even further. Also, it is worth mentioning that according to Crispin's equivalence RCS theorem [16], σ_{bi} and σ_{mono} vary over comparable values when $\beta < 180°$, meaning that one could be greater than the other depending on the scattering geometry and conditions.

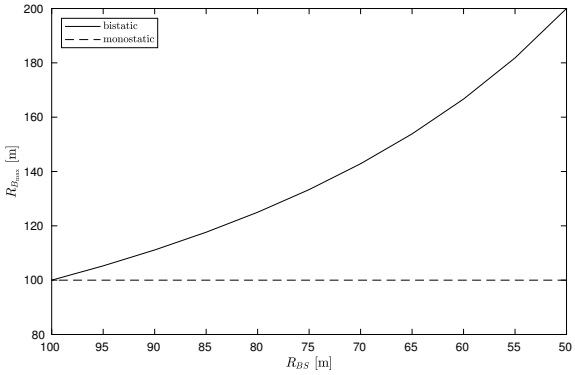

Fig. 2. Maximum detectable range: bistatic vs monostatic ($\sigma_{\text{bi}} = \sigma_{\text{mono}}$).

Let $\mathcal{R}_{\text{mono}}$ and $\mathcal{R}_{\text{bi}}$ be the maximum unambiguous bounds of R_B for monostatic and bistatic radar respectively. Knowing that $\mathcal{R}_{\text{mono}} = \frac{cf_s}{2\mu}$, using (3) and (17), we can define the following

$$\mathcal{R}_{\text{bi}} = 2\mathcal{R}_{\text{mono}} - R_{BS}. \tag{20}$$

From (20), we can see that the maximum unambiguous range of the proposed application is at least that of a monostatic radar and at most twice of it. In theory, this permits relaxing the sampling-clock requirements which can reduce the energy cost. However, setting the sampling frequency to achieve the lower bound would be a more practical approach. From (18), we can see that the resolution of the proposed application is poorer than that of a monostatic radar (typically $\frac{c}{2B}$). However, the proposed scenario offers other advantages depending on the instantaneous geometry of vehicles. For instance, when two cars have the same monostatic range from the searching vehicle but different multi-path range, they can still be separated here while monostatic radar fails. In addition, extending this proposal to deploying multiple roadside sensors with well-designed cooperative transmission protocols could improve range resolution beyond monostatic radar capabilities.

In (14) it was assumed that perfect synchronisation between car A and the roadside sensor is achieved. However, synchronisation errors may occur in reality, so we can define the

minimum requirement of time synchronisation for acceptable errors in parameter estimation. Let the synchronisation error be τ_e (in seconds), assumed constant within one frame. The de-chirped signal (16), taking into account time synchronisation error, becomes

$$\begin{aligned}&\hat{z}(m,n,l)\\&= \exp[-j2\pi(f_0\frac{\hat{R}_S}{c}+\mu\frac{\hat{R}_S}{c}\frac{n}{f_s}+f_0\frac{V_d}{c}mT+\frac{f_0 d\sin\theta_S}{c}l)]\\&+\exp[-j2\pi(f_0\frac{\hat{R}_m}{c}+\mu\frac{\hat{R}_m}{c}\frac{n}{f_s}+f_0\frac{V_m}{c}mT+\frac{f_0 d\sin\theta_B}{c}l)],\end{aligned} \tag{21}$$

where $\hat{R}_S = R_S \pm \tau_e c$ and $\hat{R}_m = R_m \pm \tau_e c$.

We can see from (21) that the synchronisation error can cause a drift in the estimated range. Intuitively, this drift in range can be considered negligible if it is smaller than half of the resolution bound. So, using (18), the maximum accepted clock offset in this proposed application can be defined as

$$\tau_{e,\max} = \max\left(\frac{1}{2B}, \frac{1}{4B\cos(\beta/2)}\right). \tag{22}$$

V. Data Processing and Parameter Estimation

The sampled data in (16) is stored into a matrix format, then two-dimensional FFT (2D-FFT) is applied for range-Doppler and range-DOA processing.

A. Range-Doppler Estimation

The raw data for fast-time and slow-time domains is stored into a 2D matrix $\mathbf{Z}_{RV} \in \mathbb{C}^{K\times M}$

$$\mathbf{Z}_{RV} = s_d \cdot \mathbf{r}_d \cdot \mathbf{v}_d^T + s_m \cdot \mathbf{r}_m \cdot \mathbf{v}_m^T + \mathbf{N}_{RV}, \tag{23}$$

where $(.)^T$ is the transpose operator, s denotes the constant complex amplitude (contains the dimensionless term $e^{-j2\pi(\frac{Rf_0}{c})}$ and the signal amplitude), $\mathbf{r}$ contains the fast-time term $e^{-j2\pi(\frac{R\mu}{c}\frac{n}{f_s})}$, $\mathbf{v}$ contains the slow-time term $e^{-j2\pi(\frac{Vf_0}{c}mT)}$, and $\mathbf{N}_{RV}$ is additive white Gaussian noise (AWGN). Computing the range-Doppler 2D-FFT allows us to estimate the peaks corresponding to (R_S, V_d) and (R_m, V_m). By applying the triangle inequality, we can state that $R_S > R_{BS}+R_B = R_m$ (assuming no reflections from objects on the LOS between the searching vehicle and the sensor). So, the peak with the smallest range corresponds to (R_S, V_d), while the remaining peak corresponds to (R_m, V_m).

B. Range-DOA Estimation

The raw data for fast-time and element domains is stored into a 2D matrix $\mathbf{Z}_{R\theta} \in \mathbb{C}^{K\times L}$

$$\mathbf{Z}_{R\theta} = s_d \cdot \mathbf{r}_d \cdot \mathbf{a}_d^T + s_m \cdot \mathbf{r}_m \cdot \mathbf{a}_m^T + \mathbf{N}_{R\theta}, \tag{24}$$

where $\mathbf{a}$ contains the element term $e^{-j2\pi(\frac{f_0 d\sin\theta}{c}l)}$ and $\mathbf{N}_{R\theta}$ is AWGN. Computing the range-DOA 2D-FFT allows us to estimate the peaks corresponding to (R_S, θ_S) and (R_m, θ_B) which can be matched directly to the corresponding range parameters previously estimated.

The estimated parameters are then stored and processed as shown in Algorithm 1.

Algorithm 1 FFT-based parameter estimation algorithm.

Require: $\mathbf{Z}_{RV}$, $\mathbf{Z}_{R\theta}$, f_0, μ

1: Apply 2D-FFT to $\mathbf{Z}_{RV}$; compute a range-Doppler map.
2: Search for the peaks in the range-Doppler map; determine R_S, V_d, R_m, and V_m.
3: Apply 2D-FFT to $\mathbf{Z}_{R\theta}$; compute a range-DOA map.
4: Search for the peaks in the range-DOA map; determine θ_S and θ_B.
5: Using θ_S and θ_B, calculate γ according to (2).
6: Using γ, R_S and R_m, calculate R_B according to (4).
7: Using V_d and θ_S, calculate v_a according to (5).
8: Using R_m, R_B, R_S, θ_B, and γ, calculate α according to (7).
9: Using V_m, v_a, θ_B, and α, calculate v_b according to (8).
10: **return** R_B v_b and θ_B.

TABLE I
Radar Settings Used in the Simulations

Parameter	Value	Parameter	Value
Transmit Power	10dBm	f_0	77GHz
Transmit Antenna Gain	23dBi	B	300MHz
Receiver Antenna Gain	16dBi	T_c	30μs
Multi-Path RCS	1dBsm	T	35μs
NF	12dB	f_s	17.07MHz
K	512	M	256
L	128	d	1.948mm

VI. Simulations

Computer simulations were conducted to verify the success of the proposed application. The roadside sensor, car A, and car B were placed at map coordinates to replicate the road scenario of Fig. 1. The one-way and two-way free-space propagation models were used to determine the power of the received direct path and multi-path, respectively. The radar system characteristics used are recommended by the International Telecommunication Union (ITU) for automotive applications in [17]. A summary of the transmitter/receiver characteristics as well as the FMCW parameters are summarised in Table I.

In the first simulation, the noise figure (NF) was fixed to 12dB (recommended in [17] for operating monostatic range up to 100m). The estimated parameters after applying Algorithm 1 are shown vs the true values in Table II. We can see that at the recommended NF of 12dB, the motion parameters can be accurately estimated in the proposed application.

Monte-Carlo simulations were also performed at different levels of noise. A scenario where car A is equipped with an equivalent monostatic radar was used as a reference. NF was varied between a range of 10-30dB, and 2000 tests were

TABLE II
True vs Estimated Parameters (NF = 12dB)

Parameter	R_S[m]	R_B[m]	v_a[m/s]	v_b[m/s]	θ_S[°]	θ_B[°]
True	51.41	92.24	13.41	15.64	-20	26.31
Estimated	51.01	92.30	13.42	15.57	-20.10	25.94

run for each level of noise. Then, the root-mean-square error (RMSE) for the estimated range, Doppler and DOA was calculated. Fig. 3 shows the results. We can see that in the proposed case (bistatic) the motion parameters for both signal paths can be accurately estimated as NF approaches the recommended levels. As expected, it outperforms the monostatic case when estimating the multi-path signal. Although the direct-path signal dominates the FFT spectrum, a simple peak search was sufficient to detect the multi-path signal. It is important to mention that more advanced peak search algorithms and direct-path suppression techniques, such as constant false alarm rate (CFAR) [18], could yield better RMSE at higher noise levels. However, such research direction is outside the scope of this work.

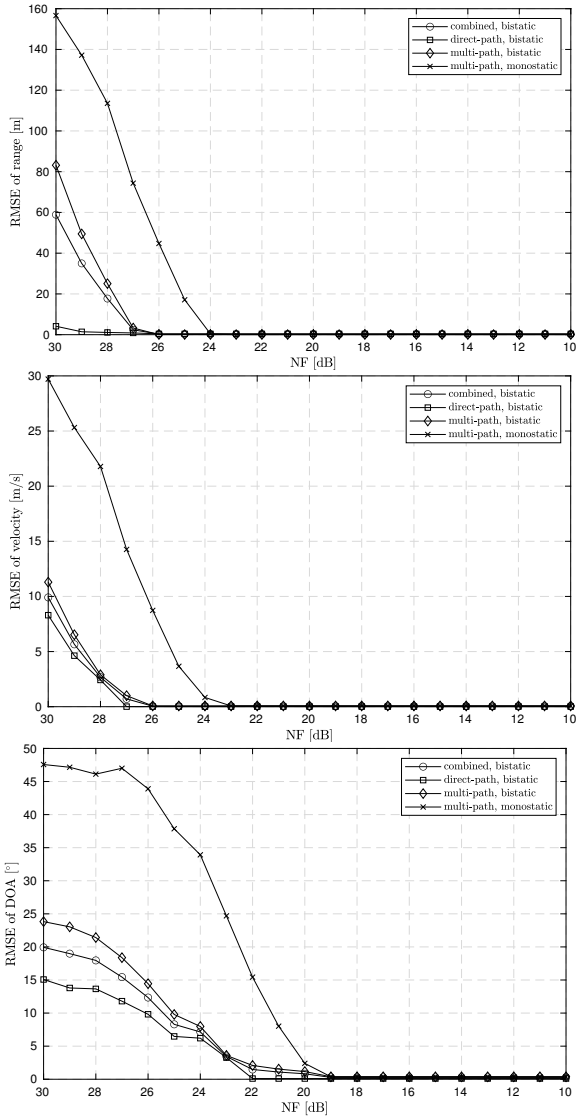

Fig. 3. A comparison of RMSE vs NF between the proposed bistatic radar application and the monostatic equivalent ($\sigma_{\text{bi}} = \sigma_{\text{mono}}$).

VII. Conclusion

An automotive application for bistatic radar was proposed employing cooperative roadside sensors. While such application can enhance the detection range of the vehicle, it can also reduce the power cost associated with the constant transmission while in autopilot mode. Although perfect synchronisation between the sensor and the searching car is a critical task, we focused here on the radar signal processing aspect and derived the general geometry of a scenario when the searching vehicle is approaching the roadside sensor while the target is receding it. It was shown that the motion parameters can be unambiguously estimated when the searching vehicle is equipped with an antenna array in the receiving mode. Computer simulations have shown that the proposed application outperforms the monostatic equivalent in considered scenarios.

References

[1] D. Grimes and T. Jones, "Automotive radar: A brief review," *Proceedings of the IEEE*, vol. 62, no. 6, pp. 804–822, 1974.

[2] S. M. Patole, M. Torlak, D. Wang, and M. Ali, "Automotive radars: A review of signal processing techniques," *IEEE Signal Processing Magazine*, vol. 34, no. 2, pp. 22–35, 2017.

[3] H. D. Griffiths and C. J. Baker, *An introduction to passive radar*. Artech House, 2017.

[4] M. E. Davis, *Advances in Bistatic Radar*. SciTech Publishing, 2007, vol. 2.

[5] J. M. Thomas, C. J. Baker, and H. D. Griffiths, "HF passive bistatic radar potential and applications for remote sensing," in *2008 New Trends for Environmental Monitoring Using Passive Systems*, 2008, pp. 1–5.

[6] L. Gürel, H. Bağcı, J.-C. Castelli, A. Cheraly, and F. Tardivel, "Validation through comparison: Measurement and calculation of the bistatic radar cross section of a stealth target," *Radio science*, vol. 38, no. 3, 2003.

[7] H. C. Zeng, P. B. Wang, J. Chen, W. Liu, L. L. Ge, and W. Yang, "A novel general imaging formation algorithm for GNSS-based bistatic sar," *Sensors*, vol. 16, no. 3, p. 294, 2016.

[8] H. C. Zeng, J. Chen, P. B. Wang, W. Yang, and W. Liu, "2-D coherent integration processing and detecting of aircrafts using GNSS-based passive radar," *Remote Sensing*, vol. 10, no. 7, 2018.

[9] X. K. Zhou, P. B. Wang, J. Chen, Z. R. Men, W. Liu, and H. C. Zeng, "A modified Radon Fourier transform for GNSS-based bistatic radar target detection," *IEEE Geoscience and Remote Sensing Letters*, pp. 1–5, 2020.

[10] H. Wymeersch, G. Seco-Granados, G. Destino, D. Dardari, and F. Tufvesson, "5G mmWave positioning for vehicular networks," *IEEE Wireless Communications*, vol. 24, no. 6, pp. 80–86, 2017.

[11] F. Liu, C. Masouros, A. P. Petropulu, H. Griffiths, and L. Hanzo, "Joint Radar and Communication Design: Applications, State-of-the-Art, and the Road Ahead," *IEEE Transactions on Communications*, vol. 68, no. 6, pp. 3834–3862, 2020.

[12] R. S. Thoma, C. Andrich, G. D. Galdo, M. Dobereiner, M. A. Hein, M. Kaske, G. Schafer, S. Schieler, C. Schneider, A. Schwind, and P. Wendland, "Cooperative Passive Coherent Location: A Promising 5G Service to Support Road Safety," *IEEE Communications Magazine*, vol. 57, no. 9, pp. 86–92, 2019.

[13] O. Kanhere, S. Goyal, M. Beluri, and T. S. Rappaport, "Target Localization using Bistatic and Multistatic Radar with 5G NR Waveform," in *2021 IEEE 93rd Vehicular Technology Conference (VTC2021-Spring)*. IEEE, 2021, pp. 1–7.

[14] J.-C. Lin, "Synchronization requirements for 5G: An overview of standards and specifications for cellular networks," *IEEE Vehicular Technology Magazine*, vol. 13, no. 3, pp. 91–99, 2018.

[15] H. Krim and M. Viberg, "Two decades of array signal processing research: the parametric approach," *IEEE Signal Processing Magazine*, vol. 13, no. 4, pp. 67–94, 1996.

[16] J. W. Crispin, *A Theoretical Method for the Calculation of the Radar Cross Sections of Aircraft and Missles*. University of Michigan, College of Engineering, Department of Electrical ..., 1959, vol. 59, no. 774.

[17] M. Series, "Systems characteristics of automotive radars operating in the frequency band 76–81 GHz for intelligent transport systems applications," *Recommendation ITU-R, M*, pp. 2057–1, 2014.

[18] H. Rohling, "Radar CFAR Thresholding in Clutter and Multiple Target Situations," *IEEE Transactions on Aerospace and Electronic Systems*, vol. AES-19, no. 4, pp. 608–621, 1983.